IOP Publishing Phys. Med. Biol. 68 (2023) 195004 https://doi.org/10.1088/1361-6560/acf55a

Physics in Medicine & Biology

IPEM Institute of Physics and Engineering in Medicine

RECEIVED
7 June 2023

REVISED
15 August 2023

ACCEPTED FOR PUBLICATION
30 August 2023

PUBLISHED
19 September 2023

PAPER

Regularized reconstruction based on joint smoothly clipped absolute deviation regularization and graph manifold learning for fluorescence molecular tomography

Jun Zhang[1,2], Gege Zhang[1,2], Yi Chen[1,2], Kang Li[1,2], Fengjun Zhao[1], Huangjian Yi[1], Linzhi Su[1,2,*] and Xin Cao (曹欣)[1,2,*]

[1] School of Information Science and Technology, Northwest University, Xi'an, Shaanxi 710127, People's Republic of China
[2] National and Local Joint Engineering Research Center for Cultural Heritage Digitization, Xi'an, Shaanxi 710127, People's Republic of China
[*] Authors to whom any correspondence should be addressed.

E-mail: likang@nwu.edu.cn, sulinzhi029@163.com and caoxin918@hotmail.com

Keywords: fluorescence molecular tomography, SCAD-GML, non-convex gradient descent iterative method, inverse problems

Abstract

Objective. Fluorescence molecular tomography (FMT) is an optical imaging modality that provides high sensitivity and low cost, which can offer the three-dimensional distribution of biomarkers by detecting the fluorescently labeled probe noninvasively. In the field of preclinical cancer diagnosis and treatment, FMT has gained significant traction. Nonetheless, the current FMT reconstruction results suffer from unsatisfactory morphology and location accuracy of the fluorescence distribution, primarily due to the light scattering effect and the ill-posed nature of the inverse problem. *Approach.* To address these challenges, a regularized reconstruction method based on joint smoothly clipped absolute deviation regularization and graph manifold learning (SCAD-GML) for FMT is presented in this paper. The SCAD-GML approach combines the sparsity of the fluorescent sources with the latent manifold structure of fluorescent source distribution to achieve more accurate and sparse reconstruction results. To obtain the reconstruction results efficiently, the non-convex gradient descent iterative method is employed to solve the established objective function. To assess the performance of the proposed SCAD-GML method, a comprehensive evaluation is conducted through numerical simulation experiments as well as *in vivo* experiments. *Main results.* The results demonstrate that the SCAD-GML method outperforms other methods in terms of both location and shape recovery of fluorescence biomarkers distribution. *Siginificance.* These findings indicate that the SCAD-GML method has the potential to advance the application of FMT in *in vivo* biological research.

1. Introduction

With the rapid development of medical imaging equipment and fluorescent probes, fluorescence molecular imaging (FMI) has increasingly used in clinical applications and the study of protein function in recent years (Ntziachristos *et al* 2003, Ntziachristos *et al* 2005, Ntziachristos 2010, Chi *et al* 2014, Hu *et al* 2020). By detecting the distribution of targeted fluorescence probes in biological tissues, FMI enables noninvasive imaging of biomarkers (Weissleder *et al* 1999, Weissleder 2002). However, FMI only provides qualitative planar photon distribution information on the surface of an imaging object, thereby restricting its effectiveness in tumors studies (Hu *et al* 2010, Mohajerani and Ntziachristos 2015, Zhang *et al* 2018). As a solution, fluorescence molecular tomography (FMT) has been proposed based on FMI. FMT is an imaging modality designed to achieve three-dimensional visualization of fluorescence regions within biological tissues *in vivo* by solving the reconstruction problem (Willmann *et al* 2008, Ale *et al* 2012). Owing to its cost-effectiveness and high sensitivity, this optical molecular modality has found wide-ranging applications in preclinical diagnostics (Ale *et al* 2012).

However, despite the promising advantages of FMT, achieving excellent reconstruction performance contionues to be a significant challenge due to the severe scattering effect of light in biological tissues and the ill-posed nature of the inverse problem (Guo *et al* 2017, Meng *et al* 2019). To address these challenges, numerous strategies have been proposed to enhance the quality of FMT reconstruction. One kind of the strategies is to incorporate structural prior knowledge. For instance, incorporating spatial distribution information from computed tomography (CT) and magnetic resonance imaging (MRI) can significantly improve the accuracy and stability of FMT (Kircher *et al* 2012, Hu *et al* 2015). In the studies of orthotopic glioma morphological FMT reconstruction, several reconstruction methods employing this strategy have been shown to effectively recover the morphology of fluorescence distribution (Schulz *et al* 2009, Davis *et al* 2013, Holt *et al* 2015). Furthermore, various optimization methods based on different regularization terms are also used to alleviate the ill-posed problem in FMT reconstruction. And various methods based on sparse regularization terms, including L_0, L_1 and $L_p(0 < p < 1)$ (Zhang *et al* 2011, Shi *et al* 2015, Edjlali and Bérubé-Lauzière 2018), have been proposed in recent years. However, the reconstruction algorithms based on these regularization methods have their drawbacks. L_0-norm regularization involves a problem of combinatory optimization, rendering it unsuitable for practical applications. L_2-norm regularization results in over-smoothing, making it challenging to obtain sharp boundaries (Cao *et al* 2007). L_1-norm regularization results in over-sparseness in reconstruction. To overcome these problems, some new methods based on joint regularization, such as sparse-graph manifold learning (SGML) (Guo *et al* 2020) and L_1-L_2 norm regulation via difference of convex algorithm (L_1-L_2 via DCA) algorithm (Zhang *et al* 2016) have been proposed.

In addition to traditional methods, deep learning strategies have been introduced to FMT reconstruction in recent years (Gao *et al* 2018, Guo *et al* 2018, Guo *et al* 2019, Du *et al* 2022). For instance, Meng *et al* presented a novel K-nearest neighbor based locally connected (KNN-LC) network for FMT reconstruction in 2020, demonstrating promising performance in terms of stability and accuracy (Meng *et al* 2020). While deep learning methods can overcome the inaccuracies associated with the photon propagation model and the ill-posed nature of the inverse problem, they are often limited by poor model generalization and time-consuming computations, which hinders their clinical applicability.

In this paper, a regularized reconstruction approach based on joint smoothly clipped absolute deviation regularization and graph manifold learning (SCAD-GML) for FMT is proposed. The proposed approach addresses the challenges of FMT reconstruction by leveraging the benefits of both SCAD regularization and GML. The SCAD regularization exploits the sparsity property of fluorescent sources and mitigates the ill-posedness of FMT reconstruction. And GML model can exploit the latent manifold structure and morphology of fluorescent source distribution, thus improving the shape similarity of reconstruction results. The combination of the SCAD regularization and GML model balances the sparseness, smoothness, and morphology for FMT reconstruction, which improves the accuracy and robustness of reconstruction results. The inverse problem of FMT reconstruction is converted into a non-convex minimization problem by using SCAD-GML method. The non-convex gradient descent iterative method (NGDIM) is used for solving the proposing optimization problem.

To assess the effectiveness of the proposed SCAD-GML method in FMT reconstruction, simulation experiments and *in vivo* experiments were conducted. L_2-based Incomplete variables truncated conjugate gradient (IVTCG) method (He *et al* 2010) and L_1-based iterative shrinkage (IS-L_1) (Han *et al* 2010) were used for comparisons. The experimental results indicated that the SCAD-GML method outperformed the other two methods in terms of both the location accuracy and shape recovery of the fluorescence biomarkers distribution. This demonstrates the significant improvement achieved by the proposed SCAD-GML method in the performance of FMT reconstruction.

The paper is organized as follows. In section 2, we introduce the FMT forward model, FMT inverse problem and the SCAD-GML method. In section 3, we introduce the process and results for both numerical simulation and *in vivo* experiments. In section 4, we make some summary and discussion of this paper.

2. Methods

Photon propagation in the near-infrared spectral band has a strongly scattering characteristic in the biological tissues. For steady-state FMT reconstruction with a point excitation source, the diffusion equation (DE) with the Robin-type boundary condition can be used to describe the propagation process of photons in the biological tissues (Lee *et al* 2007, Liu *et al* 2018). This can be expressed as follows:

$$\begin{cases} -\nabla[D_x(r)\nabla\Phi_x(r)] + \mu_{ax}(r)\Phi_x(r) = \Theta\delta(r - r_s)\ (r \in \Omega) \\ -\nabla[D_m(r)\nabla\Phi_m(r)] + \mu_{am}(r)\Phi_m(r) = \Phi_x(r)\eta\mu_{af}(r)\ (r \in \Omega) \\ 2D_{x,m}(r)\nabla\Phi_{x,m}(r) + q\Phi_{x,m}(r) = 0\ (r \in \partial\Omega) \end{cases} \tag{1}$$

where r is the location vector inside the imaging domain Ω, and r_s is the position vector of the point excitation sources with the amplitude Θ. $D_{x,m} = 1/3(\mu_{ax,am} + (1 - g)\mu_{sx,sm})$ denotes the diffusion coefficient and g is the anisotropy parameter (Jacques 2013). μ_{ax} and μ_{am} represents the absorption coefficients of excited light and emitted light, respectively. $\Phi_x(r)$ and $\Phi_m(r)$ denotes the photon flux density at position r of excited light and emitted light, respectively. μ_{af} is the fluorescent source to be reconstructed, η is quantum efficiency and q denotes the optical reflective index of the biological tissues.

$$AX = \Phi \tag{2}$$

where A denotes the system weight matrix. Φ denotes the photon segment on the surface of the measured object detected by the highly sensitive detector, and X is the spatial distribution of fluorescent sources within the biological tissues. The detail description can be found in (Wang *et al* 2009). Thus, the goal of solving the FMT inverse problem is the recovery of the fluorescent distribution X from the above linear matrix equation.

2.1. Inverse problem

FMT reconstruction is aimed at solving the inverse problem described by equation (2). However, since only the photon distribution on the surface is measurable, the dimension of the measured data is significantly lower than that of the internal fluorescence distribution. This leads to the ill-posed nature of the FMT problem, making the reconstruction process challenging. In order to ensure the stability of FMT reconstruction and preserve the details of fluorescent regions, this paper adopts SCAD regularization. By combining the SCAD regularization with the objective function of FMT reconstruction, the optimization function can be formulated as follows:

$$\frac{1}{2}\|AX - \Phi\|_2^2 + \sum_{i=1}^{n} f_\lambda(x_i) \tag{3}$$

where $\|.\|_2^2$ denotes the L_2 norm, that is, $\|\beta\|^2 = \sum_{j=1}^{d}\beta_j^2$. And $f_\lambda(x)$ is the SCAD regularization function, which can be formulated as:

$$f_\lambda(\mathrm{x}) = \begin{cases} \lambda|x|, & 0 \leqslant |x| < \lambda \\ -\dfrac{x^2 - 2a\lambda|x| + \lambda^2}{2(a-1)} & \lambda \leqslant |x| < a\lambda \\ \dfrac{(a+1)\lambda^2}{2} & \text{otherwise} \end{cases} \tag{4}$$

where λ is the nonnegative regularization parameter, a is a constant greater than 2. Fan and li used $a = 3.7$ for moderate sample size (Fan and Li 2001). We adopt it in the experiments.

To improve the morphological recovery of FMT reconstruction, the GML model is used in this paper. The complete FMT reconstruction process using SCAD-GML method can be defined as follows:

$$\frac{1}{2}\|AX - \Phi\|_2^2 + \sum_{i=1}^{n} f_\lambda(x_i) + \mu\|LX\|_2^2 \tag{5}$$

where μ is the regularization parameter, which determines the balance between the regularity term and fidelity term in the optimization process. L is the Laplacian graph matrix, which is defined as follows:

$$L_{i,j} = \begin{cases} 1 & i = j \\ -\exp\left(-\dfrac{d_{i,j}^2}{4R^2}\right)/\rho_{s_k} & i, j \in S_k,\ i \neq j \\ 0 & \text{otherwise} \end{cases} \tag{6}$$

where R denotes the radius of the Gaussian kernel function which is used to modify the probability density function of the nearby vertexes within the same organ. d_{ij} denotes the Euclidean distance between the ith and jth vertex. S_k is the vertex set in the kth organ. p_{sk} denotes the region mollifier that prevents the influence of vertex distribution variation and ensures the total edge weight in the same organ is 1. The definition is as follows:

$$\rho_{s_k} = \sum_{\forall g,l \in s_k, g \neq l} \exp\left(-\frac{d_{g,l}^2}{4R^2}\right). \tag{7}$$

Algorithm 1. SCAD-GML method for FMT Reconstruction.

Input: The detected surface photon Φ and the system matrix A.
Initialization: The initial optimal approximation solution $\widehat{x_0} = A^{+}\Phi$, the Maximum iteration number $maxIter = 600$, the regularization parameter $\lambda = 1 \times 10^{-3}$, $\mu = 1 \times 10^{-2}$, the adjustment coefficient $\gamma = 1 \times 10^{-2}$, iteration index $k = 1$.
Step1: Find the nearby vertexes in the same organ and construct the organ vertex set S_k. Calculate the region mollifier ρ_{s_k} by the vertex set S_k.
Step2: Calculate the graph Laplacian matrix L, via the equation (6).
Repeat
Step3: Referencing equation (8), calculate the gradient vector of the current function.
Step4: Update solution x_{k+1} according to the gradient vector, via equation (10). And the point less than 0 is set to 0 in x_{k+1}.
Step5: Increase the iteration index $k = k + 1$.
Until $k > maxIter$
Output: x_k.

2.2. FMT reconstruction based on the SCAD-GML method

Generally, solving equation (5) is a challenging task due to its non-convex nature and the absence of efficient optimization methods. In this paper, the NGDIM is selected to address this challenge, leveraging the principles of non-convex optimization theory. The details of the NGDIM will be explained in this section.

The NGDIM method is an optimization algorithm that shares similarities with the Newton iteration method. Its central objective is to minimize the objective function by performing gradient descent, leveraging the gradient information of the objective function to efficiently converge to the optimal solution. The gradient of equation (5) is obtained as follows:

$$A^{\mathrm{T}}(AX - \Phi) + 2\mu L^{\mathrm{T}}LX + (f'_{\lambda}(x_1), f'_{\lambda}(x_2), \cdots, f'_{\lambda}(x_n)) \tag{8}$$

where $f'_{\lambda}(x_i)$ is the gradient of the SCAD regularization function. The expression of it is as follows:

$$f'_{\lambda}(x_i) = \begin{cases} \lambda sign(x_i) & \text{if } 0 < |x_i| < \lambda \\ \dfrac{a\lambda \mathrm{sign}(x_i) - x_i}{a - 1} & \text{if } \lambda \leqslant |x_i| < a\lambda \\ 0 & \text{otherwise} \end{cases} \tag{9}$$

The iterative update formula can be derived from equation (8), as follows:

$$\begin{aligned} x_{k+1} = x_k - \gamma(A^{\mathrm{T}}(Ax_k - \Phi) + 2\mu L^{\mathrm{T}}Lx_k \\ + (f'_{\lambda}(x_1), f'_{\lambda}(x_2), \cdots, f'_{\lambda}(x_n))), \; k = 0, 1, 2 \end{aligned} \tag{10}$$

where γ is the adjustment coefficient with a value ranging from 0 to 1. Its purpose is to ensure that the solution gradually approaches the optimal solution. In the experiments, we adopt a fixed value of 0.01 for ease of calculation and implementation. By continuously iterating according to equation (10), the FMT inverse problem can be solved. Thus, Algorithm 1 outlines the main steps of the SCAD-GML method. It should be noted that the selection of parameter values in the SCAD-GML method is based on experience.

3. Experiments and results

In order to confirm and thoroughly assess the effectiveness of the SCAD-GML method in FMT reconstruction, this section offers three separate sets of numerical simulation experiments and one set of *in vivo* experiments. Specifically, the location accuracy, robustness, morphological recovery ability and practicality of SCAD-GML method were evaluated. Two other algorithms were used to compare with our proposed method, namely, IVTCG and IS-L_1. All experiments and programs were executed on a personal computer with an Intel(R) Core (TM) i5-8265 CPU (1.8 GHz) and 8GB RAM. The computational environment allowed for efficient and reliable evaluation of the proposed SCAD-GML method, as well as the comparison with the other algorithms.

3.1. Experimental process

3.1.1. Numerical simulations

The heterogeneous phantom model was used for numerical simulation experiments, and its 3D view is shown in figure 1(A). The model was a cylinder with a radius of 10 mm and a height of 30 mm, which contains five organs: heart, bone, lung, muscle, and liver. The optical parameters of these tissues and organs at 650 nm in the model are shown in table 1 (Hou *et al* 2017). In the inverse reconstruction, the model was discretized into a finite element mesh of 4626 nodes and 25840 tetrahedral elements by using Comsol Multiphysics software as shown in

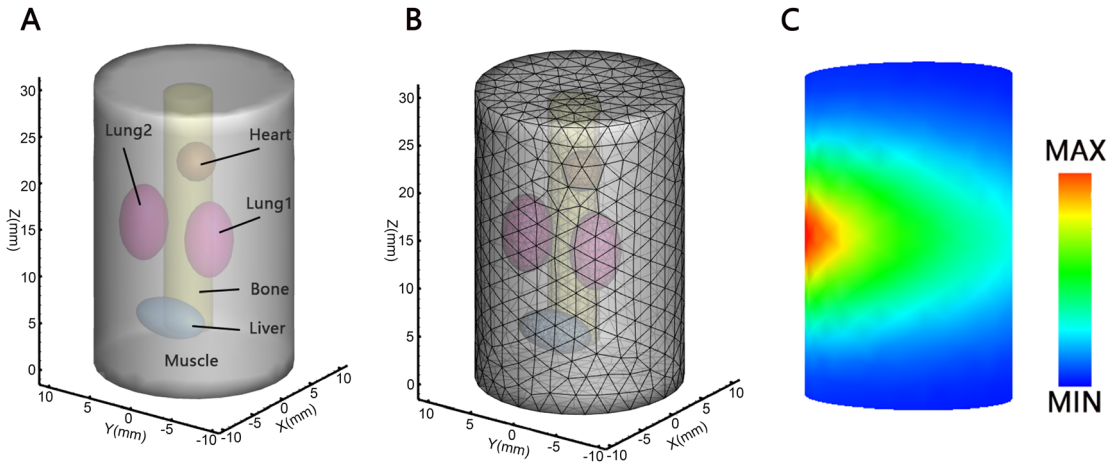

Figure 1. (A) The 3D view of the heterogeneous phantom model. (B) The finite element mesh diagram obtained by model discretization. (C) The forward simulation result of the single-source.

Table 1. The optical parameters in numerical simulation.

Tissues	$\mu_{ax}(\text{mm}^{-1})$	$\mu_{sx}(\text{mm}^{-1})$	$\mu_{am}(\text{mm}^{-1})$	$\mu_{sm}(\text{mm}^{-1})$	g
Muscle	0.0052	10.80	0.0068	10.30	0.90
Heart	0.0083	6.73	0.0104	6.60	0.85
Bone	0.0060	60.09	0.0030	30.74	0.90
Liver	0.0329	7.00	0.0176	6.60	0.90
Lungs	0.0133	19.70	0.0203	19.50	0.90

figure 1(B). (Parvitte *et al* 2013). Figure 1(C) is the forward simulation result, which was generated by the molecular optical simulation environment (MOSE) based on the Monte Carlo method (Ren *et al* 2010). This model was used to simulate the realistic optical properties and geometry of biological tissues, allowing for accurate assessment of the performance of the SCAD-GML algorithm in a controlled and reproducible environment.

Three groups of simulation experiments were completed in the heterogeneous phantom model. In the single-source simulation experiment, a uniform sphere light source with a radius of 1 mm and a center at (6 mm, 6 mm, 22 mm) was used to simulate the actual fluorescent source. In the dual-source simulation experiment, two uniform sphere lights with a radius of 1 mm at (−6 mm, 5 mm, 13 mm) and (−6 mm, 5 mm, 18 mm) centers were used to simulate two actual fluorescent sources. These simulation experiments were designed to evaluate the performance of the SCAD-GML method in terms of shape recovery accuracy and spatial positioning accuracy in the model. Moreover, a series of anti-noise simulation experiments were conducted to evaluate the robustness of the SCAD-GML method. Specifically, 5%, 10%, 15%, 20%, 25% Gaussian noise was added to the single-source simulation experiment.

3.1.2. In vivo experiment

To further assess the practical performance of the SCAD-GML method, *in vivo* experiment was conducted following the approved protocols of the Animal Ethics Committee of the Northwest University of China and Use Committee. The experiment utilized an adult BALB/c mouse, and a dual-modality FMT/CT imaging system was employed to acquire CT images and fluorescence images. The transmissive FMT was used in the dual-modality imaging system. The transmissive FMT has the advantage of being more suitable for tomographic imaging of targets located deep within the tissue and is less susceptible to excitation light leakage compare to reflective FMT (Darne *et al* 2013). The system diagram is shown in figure 2, and the detailed experimental procedure was as follows.

In the initial step, a spherical fluorescent bead with a radius of 1 mm, containing Cy5.5 solution was implanted into the abdominal cavity of the mouse, serving as the fluorescence target. The fluorescent bead was encased in a plastic material, facilitating its detection using CT for precise localization of the actual fluorescent region. After that, the mouse was fixed vertically on the rotation platform and remained stationary during the imaging process by administering anesthesia through inhalation of isoflurane gas. After a six-hour interval, a 680 nm continuous wave semiconductor laser was employed to provide the excitation illumination. Subsequently, a

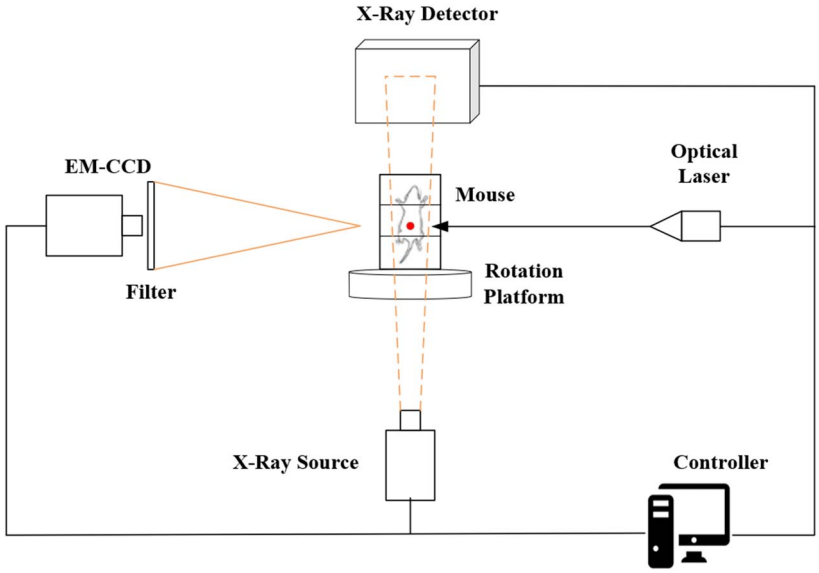

Figure 2. The prototype FMT imaging system.

thermoelectric-cooled electron multiplying charge-coupled device (EM-CCD) camera (−80, iXonEM+888) with a 120° field of view captured the surface fluorescence image, with an exposure time set at 1 s. To filter out noise, an appropriate 750 ± 10 nm bandpass filter was used to capture and confine the emission light. During the process of optical signal acquisition, the CCD camera captures an optical image after every 90 degrees of rotation of the rotating platform. The optical images collected are used for subsequent 3D reconstruction processes. After the acquirement of fluorescence image, CT imaging was performed on each mouse using a CT system. This step aimed to obtain structural data of the mouse, which provides detailed information about the anatomical features and tissues. After completing the data collection stage, data processing was carried out. A landmarks-based rigid-body registration method was employed to align the CT data with the fluorescence imaging. Following the registration, the absolute irradiance distribution in the two-dimensional fluorescence images was projected onto the three-dimensional surface of the mouse model. The major organs, including the muscle, skull, and brain were segmented using the Amria 5.2 software. Following segmentation, the mouse model was discretized into 6325 nodes and 29479 tetrahedral elements for FMT reconstruction. To evaluate the practicality of the SCAD-GML method *in vivo*, two other algorithms mentioned earlier were employed for comparative analysis.

3.1.3. Evaluation metrics

To rigorously quantify and analyze the location accuracy and shape recovery ability of the FMT reconstruction, this study utilized two commonly used evaluation metrics, namely the location error (LE) and the Dice coefficient (DICE).

The LE is defined as the Euclidean distance between the reconstructed fluorescent source center $(x,\ y,\ z)$ and the actual fluorescent source center $(x_0,\ y_0,\ z_0)$. It is a quantitative measure used to evaluate the positioning accuracy of the reconstruction results. The LE values are always greater than 0, and a smaller LE value signifies a higher level of accuracy in localizing the fluorescence biomarker.

$$\mathrm{LE} = \sqrt{(x - x_0)^2 + (y - y_0)^2 + (z - z_0)^2} \tag{11}$$

To verify the morphological recovery ability of the algorithm, the Dice coefficient (DICE) is used as an indicator. It measures the degree of overlap between the reconstructed fluorescent source region X and the actual source region Y. The DICE values range from 0 to 1, and the larger the value is, the greater the similarity between the reconstructed and the actual fluorescent regions, indicating a higher level of morphological recovery ability of the algorithm.

$$\mathrm{Dice} = \frac{2|X \cap Y|}{|X| + |Y|} \tag{12}$$

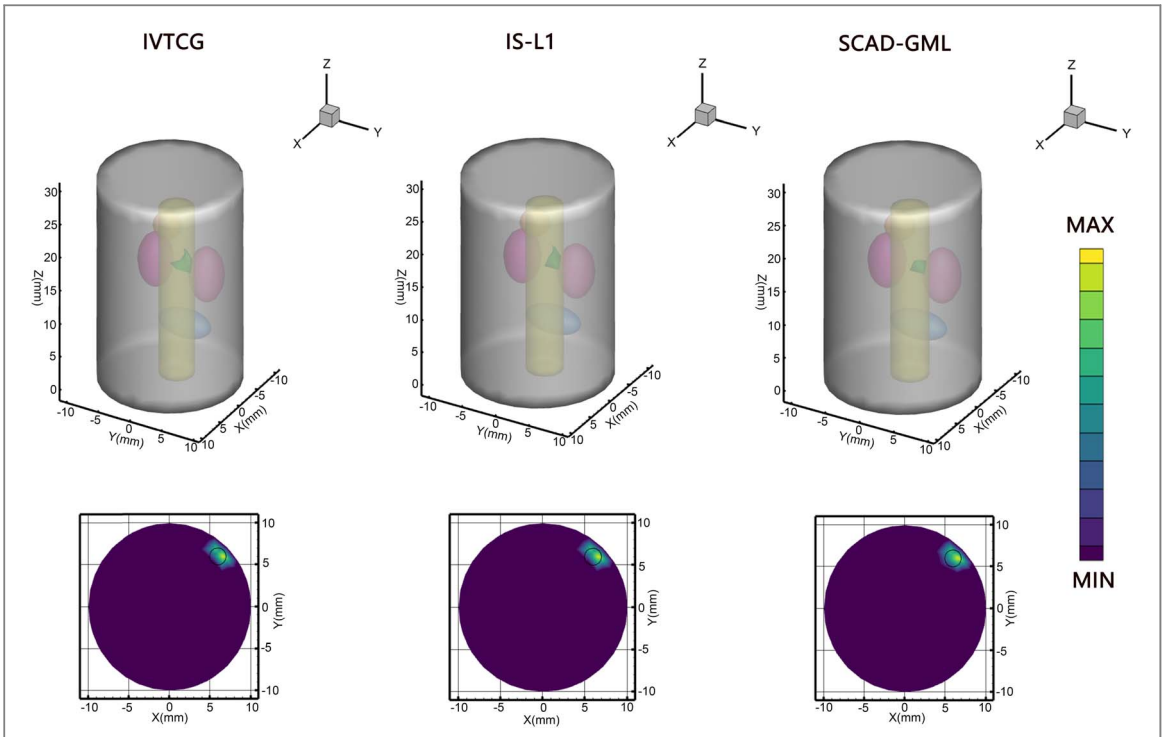

Figure 3. The 3D view of reconstruction results of single-source reconstructed by different methods. The reconstruction result is sliced along the *z*-axis of the source to obtain the axial view, and the actual source's location and size are indicated by a black circle on the plan.

Table 2. Quantitative analysis of single-source simulation reconstruction results.

Method	Actual source center (mm)	LE (mm)	DICE
IVTCG		0.741	0.399
IS-L_1	(6, 6, 22)	0.401	0.466
SCAD-GML		0.280	0.565

3.2. Results

3.2.1. Single-source simulation reconstruction

To validate the shape recovery capability of the SCAD-GML algorithm, we conducted a comparison of its performance with the IVTCG and IS-L_1 algorithms in the single-source experiment. The reconstruction results are shown in figure 3. The reconstructed fluorescent source is visualized as a green area in the three-dimensional view, and as a cyan area in the axial view. While the actual fluorescent source is represented by a black circle. It can be observed from the figure that the source reconstructed by our method overlaps most with the actual source. The quantitative analysis of the three methods is shown in table 2. According to the results in table 2, the SCAD-GML method achieved a smaller LE compared to the other methods, indicating that the reconstructed fluorescent source center was closer to the actual value. Additionally, the DICE score of the SCAD-GML method was higher, indicating a better overlap between the reconstructed and actual source regions. This is consistent with our observation.

3.2.2. Dual-source simulation reconstruction

To further assess the positioning accuracy, we contrasted the SCAD-GML algorithm's performance with the above two algorithms on the dual-source experiment. The reconstruction results of the three methods for the dual-source experiment are shown in figure 4. It is evident that the SCAD-GML method provides the most accurate reconstruction results, with better representation of the actual fluorescent source regions and more accurate center position. The quantitative analysis of the reconstruction results using the three methods is presented in table 3. The experimental results demonstrate that the SCAD-GML method outperforms the IVTCG and IS-L_1 method, achieving the lowest location error and the highest source shape recovery ability as measured by the dice coefficient. These experiment results further support the superior performance of the SCAD-GML method in terms of positioning accuracy and shape recovery in FMT reconstruction.

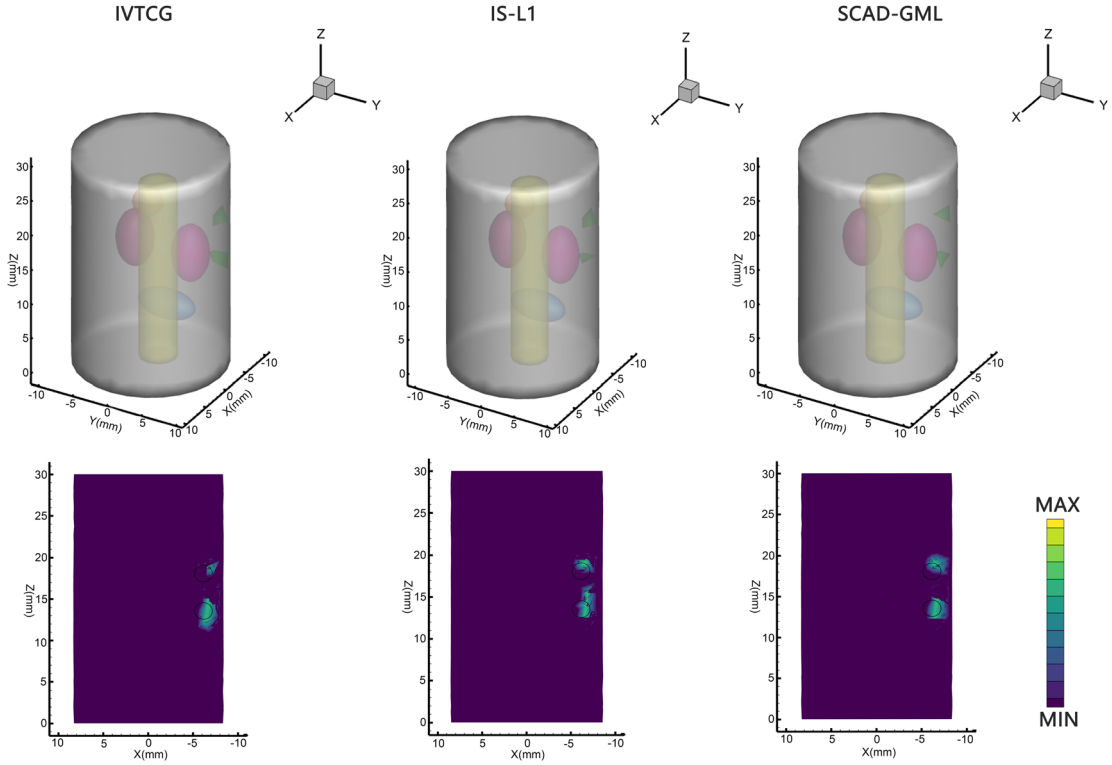

Figure 4. The reconstruction results of dual-source simulation experiment. Three different methods to reconstruct the fluorescent source are displayed in 3D view and axial view. In 3D view, the green region is the double fluorescent source of reconstruction, and in the axial view, the location and size of the real source are depicted by black circles.

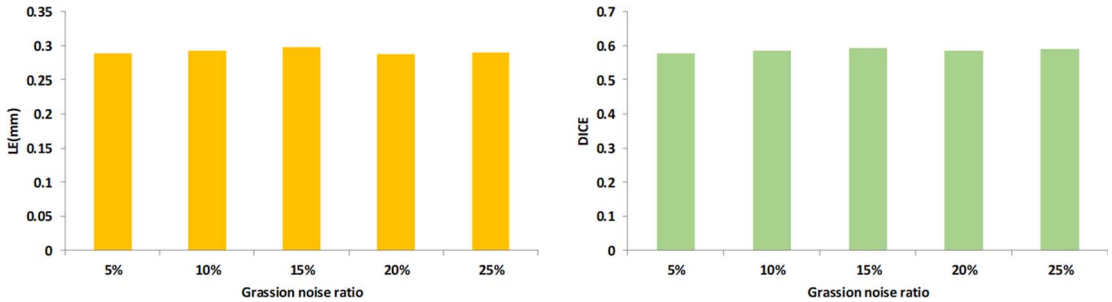

Figure 5. The results of quantitative analysis of anti-noise experiment.

Table 3. Quantitative analysis of dual-source simulation reconstruction results.

Method	Actual source center (mm)	LE (mm)	Total LE (mm)	DICE
IVTCG	(−6, 5, 13)	1.038	1.990	0.432
	(−6, 5, 18)	0.952		0.475
IS-L_1	(−6, 5, 13)	0.646	1.301	0.539
	(−6, 5, 18)	0.655		0.556
SCAD-GML	(−6, 5, 13)	0.576	1.155	0.622
	(−6, 5, 18)	0.579		0.615

3.2.3. Anti-noise performance

To assess the robustness of the SCAD-GML method, we conducted an anti-noise experiment. Specifically, we used the single-source simulation experiment to investigate the impact of adding 5%, 10%, 15%, 20% and 25%

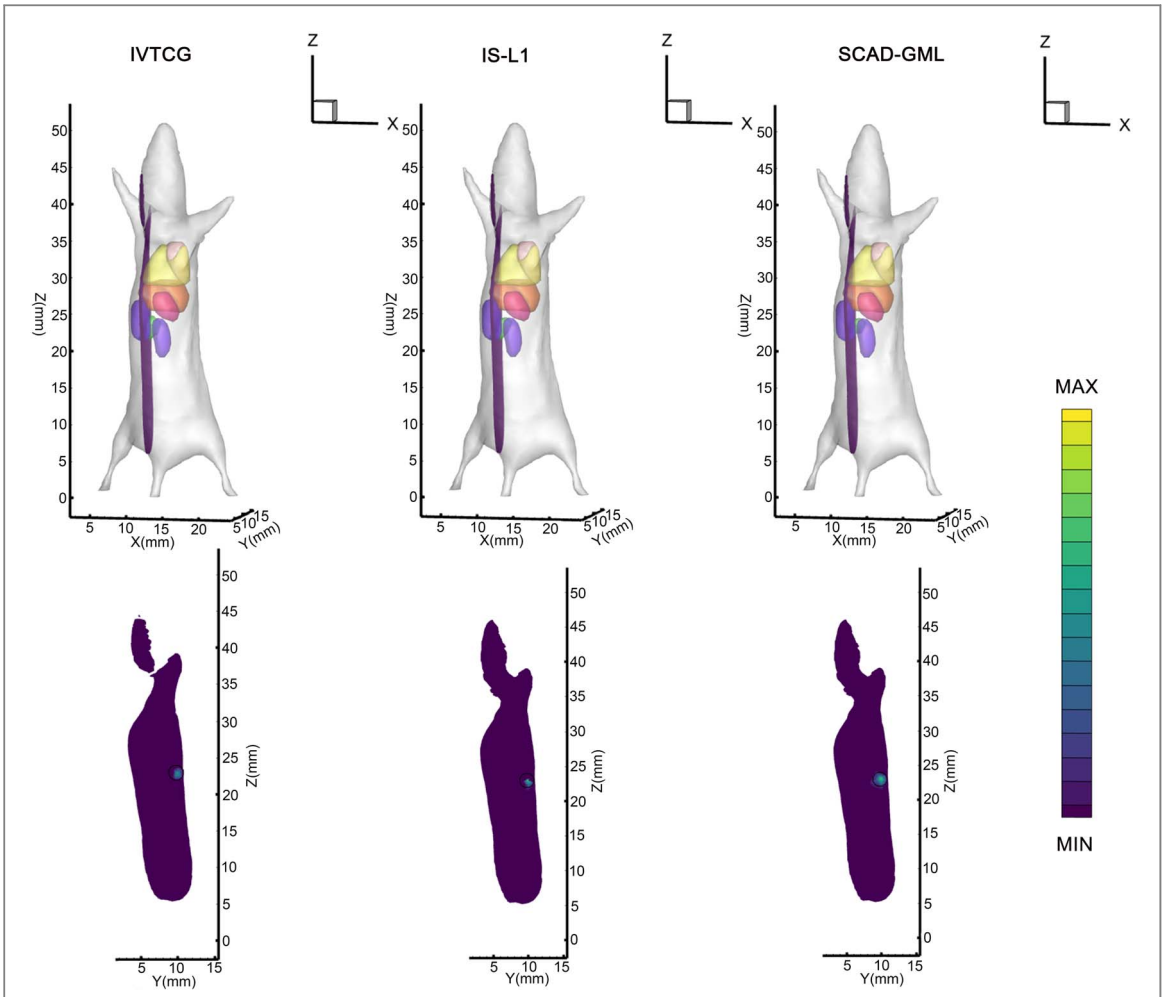

Figure 6. Results of three different reconstruction algorithms used in *in vivo* imaging experiments. The purple area in the 3D viewing angle represents the cutting surface, and the axial viewing plane below is obtained after the cutting plane is expanded, and the actual source's location and size are indicated by a black circle in the axial view.

Table 4. Quantitative analysis of *in vivo* imaging reconstruction results.

Actual source center (mm)	Method	LE (mm)	DICE
(11.5, 9.5, 22.6)	IVTCG	0.696	0.397
	IS-L_1	0.312	0.503
	SCAD-GML	0.121	0.571

Gaussian noise on the reconstruction results. As illustrated in figure 5, the fluctuation of the LE, and DICE values is negligible, indicating the method has good robustness.

3.2.4. In vivo *imaging experiment*

To assess the feasibility of the SCAD-GML method *in vivo*, we conducted an *in vivo* imaging experiment using an adult BALB/c nude mouse. The reconstruction results obtained by three methods are shown in figure 6. The quantitative analysis of the *in vivo* imaging experiment is presented in table 4. The experiments demonstrate that the SCAD-GML method has smallest LE and the largest DICE value, indicating that the SACD-GML method have superior performance in FMT reconstruction *in vivo*.

4. Discussion and conclusion

FMT is a promising imaging technology that can achieve 3D visualization of fluorescence regions in biological tissues *in vivo* at a low cost. In clinical applications, FMT can be combined with other imaging modalities to

enhance its spatial resolution. Integrating FMT with structural imaging techniques such as MRI or x-ray CT enables the fusion of molecular information with high-definition anatomical reference, leveraging prior knowledge on tissue's optical properties to improve resolution and sensitivity simultaneously (An *et al* 2015, Baikejiang *et al* 2017). In recent years, FMT has been used in tumor imaging and drug development, for example, Torres *et al* used FMT for lymph node assessment to make treatment decisions for tumors such as breast cancer and melanoma (Torres *et al* 2019). Kossodo *et al* applied FMT to drug development for cancer detection and treatment monitoring (Kossodo *et al* 2010). These preclinical studies will promote the clinical application of FMT.

However, due to the severe scattering effect of light in biological tissue and the ill-posed inverse problem, the accuracy of FMT has been limited in many biomedical applications. To improve the quality of 3D reconstruction, an effective FMT reconstruction method based on SCAD-GML method is proposed in this paper. The SCAD norm is specifically designed to strike a balance between not excessively penalizing large-valued coefficients, unlike the L1 norm, while approaching the desirable sparsity achieved by the L0 norm (Mehranian *et al* 2013). Therefore, employing SCAD regularization in FMT reconstruction yields sparser and more accurate solutions compared to using L0 or L1 regularization alone, resulting in improved FMT reconstruction accuracy. However, it is important to note that increasing sparsity in reconstruction results may lead to potential loss of morphological details (Guo *et al* 2020). Inspired by graph-based manifold learning and sparse representation theory, we propose a novel approach called SCAD-GML for regularized FMT reconstruction. The SCAD-GML method incorporates the Laplace graph model into a non-convex sparse constraint based on the SCAD norm, leveraging the latent manifold structure and morphology of the fluorescent source distribution to achieve accurate morphological recovery capability. The SCAD-GML method combines the SCAD regularization and GML to balance the sparsity, smoothness, and morphology of fluorescent region. And a non-convex objective function is constructed by SCAD-GML method, which is then solved using the NGDIM. With these approaches, the proposed SCAD-GML method can reconstruct the characteristics of the fluorescent regions accurately and effectively.

To verify the effectiveness of the proposed SCAD-GML method, a series of numerical experiments and *in vivo* experiments were conducted, and the results were compared with two commonly used reconstruction methods (IVTCG and IS-L_1). The experimental results show that: (1) dual-source simulation experiments demonstrate that the SCAD-GML method ensures a high level of accuracy in reconstruction localization. (2) *In vivo* experiments demonstrate the feasibility of the SCAD-GML method in biomedical research. (3) The anti-noise experimental results demonstrate that the SCAD-GML method is robust to noise. (4) All experiments demonstrate that the SCAD-GML method could obtain more accurate reconstruction results than the other two methods.

While the SCAD-GML method shows good performance in FMT reconstruction, it still has some limitations. Firstly, the parameters used in the proposed method were selected based on experience. It is necessary to propose an adaptive parameter selection algorithm to choose these parameters. Furthermore, additional research is necessary to explore the clinical application of FMT using the SCAD-GML method, which will also be a focus of our future research. By addressing these limitations, the proposed SCAD-GML method could be further improved and more widely applicable in biomedical imaging research.

In summary, the proposed SCAD-GML method is an effective solution to the FMT inverse problem. It achieved better reconstruction performance in terms of both location accuracy and morphological recovery compared with the traditional methods mentioned above. In addition, it exhibits strong robustness in the FMT reconstruction. The method has great potential to enhance reconstruction performance and promote the application of FMT in *in vivo* biological studies.

Acknowledgments

This work was supported in part by National Natural Science Foundation of China (61701403,61806164); Key Research and Development Program of Shaanxi Province (2019GY215, 2021ZDLSF06-04); China Postdoctoral Science Foundation (2018M643719); Graduate Innovation Program of Northwest University (CX2023185).

Data availability statement

The data cannot be made publicly available upon publication because they are not available in a format that is sufficiently accessible or reusable by other researchers. The data that support the findings of this study are available upon reasonable request from the authors.

ORCID iDs

Xin Cao (曹欣) https://orcid.org/0000-0003-3560-6523

References

Ale A, Ermolayev V, Herzog E, Cohrs C, De Angelis M H and Ntziachristos V 2012 FMT-XCT: in vivo animal studies with hybrid fluorescence molecular tomography–x-ray computed tomography *Nat. Methods* **9** 615–20

An Y, Liu J, Zhang G, Ye J, Du Y, Mao Y, Chi C and Tian J 2015 A novel region reconstruction method for fluorescence molecular tomography *IEEE Trans. Biomed. Eng.* **62** 1818–26

Baikejiang R, Zhao Y, Fite B Z, Ferrara K W and Li C 2017 Anatomical image-guided fluorescence molecular tomography reconstruction using kernel method *J. Biomed. Opt.* **22** 055001

Cao N, Nehorai A and Jacob M 2007 Image reconstruction for diffuse optical tomography using sparsity regularization and expectation-maximization algorithm *Opt. Express* **15** 13695–708

Chi C, Du Y, Ye J, Kou D, Qiu J, Wang J, Tian J and Chen X 2014 Intraoperative imaging-guided cancer surgery: from current fluorescence molecular imaging methods to future multi-modality imaging technology *Theranostics* **4** 1072

Darne C, Lu Y and Sevick-Muraca E M 2013 Small animal fluorescence and bioluminescence tomography: a review of approaches, algorithms and technology update *Phys. Med. Biol.* **59** R1

Davis S C, Samkoe K S, Tichauer K M, Sexton K J, Gunn J R, Deharvengt S J, Hasan T and Pogue B W 2013 Dynamic dual-tracer MRI-guided fluorescence tomography to quantify receptor density in vivo *Proc. Natl Acad. Sci.* **110** 9025–30

Du M, Chen Y, Li W, Su L, Yi H, Zhao F, Li K, Wang L and Cao X 2022 MSCN-NET: multi-stage cascade neural network based on attention mechanism for Čerenkov luminescence tomography *J. Appl. Phys.* **132**

Edjlali E and Bérubé-Lauzière Y 2018 Lq− Lp optimization for multigrid fluorescence tomography of small animals using simplified spherical harmonics *J. Quant. Spectrosc. Radiat. Transfer* **205** 163–73

Fan J and Li R 2001 Variable selection via nonconcave penalized likelihood and its oracle properties *J. Am. Stat. Assoc.* **96** 1348–60

Gao Y, Wang K, An Y, Jiang S, Meng H and Tian J 2018 Nonmodel-based bioluminescence tomography using a machine-learning reconstruction strategy *Optica* **5** 1451–4

Guo H, Gao L, Yu J, He X, Wang H, Zheng J and Yang X 2020 Sparse-graph manifold learning method for bioluminescence tomography *J. Biophoton.* **13** e201960218

Guo H, He X, Liu M, Zhang Z, Hu Z and Tian J 2017 Weight multispectral reconstruction strategy for enhanced reconstruction accuracy and stability with Cerenkov luminescence tomography *IEEE Trans. Med. Imaging* **36** 1337–46

Guo H, Yu J, Hu Z, Yi H, Hou Y and He X 2018 A hybrid clustering algorithm for multiple-source resolving in bioluminescence tomography *J. Biophoton.* **11** e201700056

Guo L, Liu F, Cai C, Liu J and Zhang G 2019 3D deep encoder–decoder network for fluorescence molecular tomography *Opt. Lett.* **44** 1892–5

Han D, Tian J, Zhu S, Feng J, Qin C, Zhang B and Yang X 2010 A fast reconstruction algorithm for fluorescence molecular tomography with sparsity regularization *Opt. Express* **18** 8630–46

He X, Liang J, Wang X, Yu J, Qu X, Wang X, Hou Y, Chen D, Liu F and Tian J 2010 Sparse reconstruction for quantitative bioluminescence tomography based on the incomplete variables truncated conjugate gradient method *Opt. Express* **18** 24825–41

Holt R W, Demers J-L H, Sexton K J, Gunn J R, Davis S C, Samkoe K S and Pogue B W 2015 Tomography of epidermal growth factor receptor binding to fluorescent Affibody in vivo studied with magnetic resonance guided fluorescence recovery in varying orthotopic glioma sizes *J. Biomed. Opt.* **20** 026001

Hou Y, Hua X, Xin C, Zhang H, Xuan Q and He X 2017 Single-view enhanced cerenkov luminescence tomography based on sparse bayesian learning *Acta Optica Sinica* 12001–9

Hu Z, Fang C, Li B, Zhang Z, Cao C, Cai M, Su S, Sun X, Shi X and Li C 2020 First-in-human liver-tumour surgery guided by multispectral fluorescence imaging in the visible and near-infrared-I/II windows *Nat. Biomed. Eng.* **4** 259–71

Hu Z, Liang J, Yang W, Fan W, Li C, Ma X, Chen X, Ma X, Li X and Qu X 2010 Experimental Cerenkov luminescence tomography of the mouse model with SPECT imaging validation *Opt. Express* **18** 24441–50

Hu Z, Qu Y, Wang K, Zhang X, Zha J, Song T, Bao C, Liu H, Wang Z and Wang J 2015 *In vivo* nanoparticle-mediated radiopharmaceutical-excited fluorescence molecular imaging *Nat. Commun.* **6** 7560

Jacques S L 2013 Optical properties of biological tissues: a review *Phys. Med. Biol.* **58** R37

Kircher M F, De La Zerda A, Jokerst J V, Zavaleta C L, Kempen P J, Mittra E, Pitter K, Huang R, Campos C and Habte F 2012 A brain tumor molecular imaging strategy using a new triple-modality MRI-photoacoustic-Raman nanoparticle *Nat. Med.* **18** 829–34

Kossodo S, Pickarski M, Lin S-A, Gleason A, Gaspar R, Buono C, Ho G, Blusztajn A, Cuneo G and Zhang J 2010 Dual in vivo quantification of integrin-targeted and protease-activated agents in cancer using fluorescence molecular tomography (FMT) *Mole. Imaging Biol.* **12** 488–99

Lee J H, Joshi A and Sevick-Muraca E M 2007 Fully adaptive finite element based tomography using tetrahedral dual-meshing for fluorescence enhanced optical imaging in tissue *Opt. Express* **15** 6955–75

Liu Y, Jiang S, Liu J, An Y, Zhang G, Gao Y, Wang K and Tian J 2018 Reconstruction method for fluorescence molecular tomography based on L1-norm primal accelerated proximal gradient *J. Biomed. Opt.* **23** 085002

Mehranian A, Rad H S, Rahmim A, Ay M R and Zaidi H 2013 Smoothly clipped absolute deviation (SCAD) regularization for compressed sensing MRI using an augmented Lagrangian scheme *Magn. Reson. Imaging* **31** 1399–411

Meng H, Gao Y, Yang X, Wang K and Tian J 2020 K-nearest neighbor based locally connected network for fast morphological reconstruction in fluorescence molecular tomography *IEEE Trans. Med. Imaging* **39** 3019–28

Meng H, Wang K, Gao Y, Jin Y, Ma X and Tian J 2019 Adaptive gaussian weighted laplace prior regularization enables accurate morphological reconstruction in fluorescence molecular tomography *IEEE Trans. Med. Imaging* **38** 2726–34

Mohajerani P and Ntziachristos V 2015 An inversion scheme for hybrid fluorescence molecular tomography using a fuzzy inference system *IEEE Trans. Med. Imaging* **35** 381–90

Ntziachristos V 2010 Going deeper than microscopy: the optical imaging frontier in biology *Nat. Methods* **7** 603–14

Ntziachristos V, Bremer C and Weissleder R 2003 Fluorescence imaging with near-infrared light: new technological advances that enable *in vivo* molecular imaging *Eur. Radiol.* **13** 195–208

Ntziachristos V, Ripoll J, Wang L V and Weissleder R 2005 Looking and listening to light: the evolution of whole-body photonic imaging *Nat. Biotechnol.* **23** 313–20

Parvitte B, Risser C, Vallon R and Zéninari V 2013 Quantitative simulation of photoacoustic signals using finite element modelling software *Appl. Phys.*B **111** 383–9
Ren N, Liang J, Qu X, Li J, Lu B and Tian J 2010 GPU-based Monte Carlo simulation for light propagation in complex heterogeneous tissues *Opt. Express* **18** 6811–23
Schulz R B, Ale A, Sarantopoulos A, Freyer M, Soehngen E, Zientkowska M and Ntziachristos V 2009 Hybrid system for simultaneous fluorescence and x-ray computed tomography *IEEE Trans. Med. Imaging* **29** 465–73
Shi J, Liu F, Zhang J, Luo J and Bai J 2015 Fluorescence molecular tomography reconstruction via discrete cosine transform-based regularization *J. Biomed. Opt.* **20** 055004
Torres V C, Sinha L, Li C, Tichauer K M and Brankov J G 2019 *IEEE 16th Int. Symp. on Biomedical Imaging (ISBI 2019),2019), vol Series): IEEE)* pp 507–11
Wang D, Liu X, Chen Y and Bai J 2009 A novel finite-element-based algorithm for fluorescence molecular tomography of heterogeneous media *IEEE Trans. Inf. Technol. Biomed.* **13** 766–73
Weissleder R 2002 Scaling down imaging: molecular mapping of cancer in mice *Nat. Rev. Cancer* **2** 11–8
Weissleder R, Tung C-H, Mahmood U and Bogdanov A 1999 In vivo imaging of tumors with protease-activated near-infrared fluorescent probes *Nat. Biotechnol.* **17** 375–8
Willmann J K, Van Bruggen N, Dinkelborg L M and Gambhir S S 2008 Molecular imaging in drug development *Nat. Rev. Drug Discovery* **7** 591–607
Zhang H, Geng G, Wang X, Qu X, Hou Y and He X 2016 Fast and robust reconstruction for fluorescence molecular tomography via regularization *BioMed Res. Int.* **2016** 5065217
Zhang Q, Zhao H, Chen D, Qu X, Chen X, He X, Li W, Hu Z, Liu J and Liang J 2011 Source sparsity based primal-dual interior-point method for three-dimensional bioluminescence tomography *Opt. Commun.* **284** 5871–6
Zhang S, Ma X, Wang Y, Wu M, Meng H, Chai W, Wang X, Wei S and Tian J 2018 Robust reconstruction of fluorescence molecular tomography based on sparsity adaptive correntropy matching pursuit method for stem cell distribution *IEEE Trans. Med. Imaging* **37** 2176–84